Systems & Control Letters 215 (2026) 106472

Contents lists available at ScienceDirect

Systems & Control Letters

journal homepage: www.elsevier.com/locate/sysconle

Optimal damping in decentralized formation control☆

Erica Salvato [a,*], Alberto Trevisan [a], Franco Blanchini [b], Felice Andrea Pellegrino [a], Gianfranco Fenu [a]

[a] Department of Engineering and Architecture, University of Trieste, Trieste, Italy
[b] Department of Mathematics, Computer Science and Physics, University of Udine, Udine, Italy

ARTICLE INFO

Keywords:
Decentralized control
Formation control
Optimal damping
Impedance matching

ABSTRACT

We address the problem of formation control in multi-agent systems tasked with tracking a leader-imposed trajectory. Inter-agent interactions are encoded by a graph, with each node representing an agent that uses only relative position and velocity information from its neighbors for control. A subset of agents, designated as dampers, also utilizes their absolute velocity to improve damping in the formation. We formulate an optimization problem to minimize the maximum real part of the closed-loop eigenvalues, a criterion that directly governs both stability margins and the rate at which the formation recovers from disturbances. We derive an explicit solution for a line graph configuration where the leader and a damper occupy the endpoints. We also provide the globally optimal solution for a generic graph, assuming that each agent applies a damping action that must be the same across all nodes. We prove the overall robustness of the protocol against network topology variations. Theoretical findings are validated through both simulations and real-world experiments with a quadrotor swarm, which confirm that damping agents significantly improve formation integrity under dynamic conditions.

1. Introduction

The coordination of autonomous multi-agent systems has gained increasing attention due to its broad applicability in robotics, transportation, and surveillance [1]. In particular, formation control—where agents maintain prescribed spatial relationships while tracking a collective motion—serves as a foundational problem in distributed robotics [2]. Formation control has a long history, dating back to the '60s, when one of the first control schemes for vehicle platoons was proposed [3], addressing optimal error regulation in linear, sequentially connected systems. Over subsequent decades, the problem has been generalized beyond platoons, with emphasis on robustness, scalability, and communication constraints. This progression has established decentralized and distributed control as the dominant paradigm for large formations (see [4–6] for an overview of the subject). A key motivation for decentralization is that global control from a central unit becomes impractical as the number of agents grows or as communication becomes unreliable. Consequently, decentralized strategies [7] that rely on local control laws and relative measurements with neighboring agents have been widely studied. Depending on the sensing capabilities and interaction topologies (typically modeled as a graph), different kinds of formation control formulation can be stated [8–12] which can further be categorized according to the agents' dynamics (e.g., first/second order point-mass model or rigid body dynamics). Among the various scenarios, leader–follower configurations are especially relevant for structured group behaviors, such as those seen in aerial swarms or ground convoys. In these settings, a designated leader dictates the global trajectory, while the remaining agents coordinate locally to preserve formation and follow the intended path. A substantial body of work frames the leader–follower problem within the consensus paradigm [13]. Indeed, by properly selecting the states over which consensus is achieved, a variety of formation control problems can be reformulated as consensus problems (see, for instance [14] that deals with second order dynamics). A persistent challenge in decentralized formation control is managing the dynamic interactions that emerge from graph topology and local control laws. These interactions determine both stability margins and transient performance. In particular, disturbances or abrupt leader maneuvers can propagate

☆ This study was carried out within the PNRR research activities of the consortium iNEST (Interconnected North-Est Innovation Ecosystem) funded by the European Union Next-GenerationEU (Piano Nazionale di Ripresa e Resilienza (PNRR) – Missione 4 Componente 2, Investimento 1.5 – D.D. 1058 23/06/2022, ECS_00000043). This manuscript reflects only the Authors' views and opinions, neither the European Union nor the European Commission can be considered responsible for them.

* Corresponding author.
E-mail address: ERICA.SALVATO@dia.units.it (E. Salvato).

https://doi.org/10.1016/j.sysconle.2026.106472
Received 23 December 2025; Received in revised form 26 March 2026; Accepted 11 May 2026
Available online 2 June 2026

and amplify through the network, degrading formation integrity [7]. A widely adopted mechanism to counteract this phenomenon is the introduction of damping [15–17]. In the case of second-order dynamics, damping naturally appears as a parameter in the agents' dynamics, typically associated with the relative velocities of neighboring agents. Additionally, *damping agents*—special nodes equipped with absolute velocity measurements—can be introduced into the formation (see, e.g., [18–20]). These agents help mitigate oscillations and improve convergence without requiring centralized information. However, the optimal deployment and tuning of damping actions remain largely open questions, particularly in sparse, low-degree networks such as line or ring topologies.

The present paper addresses the problem of formation control for agents evolving on a connected graph, where only a subset may act as dampers using absolute speed feedback. Each agent implements a decentralized control strategy based solely on its relative position and velocity with respect to adjacent agents. We study the spectral properties of the closed-loop system and propose a principled approach for tuning the control parameters to minimize the maximum real part of the eigenvalues, thereby enhancing both stability and convergence speed. For line graphs—a canonical topology in many real-world systems—we provide an explicit solution for the optimal gains when the leader and damper occupy opposite ends of the formation. The main contributions of the manuscript are summarized next.

- We consider a linear decentralized control strategy that distinguishes three categories of agents: leader, regular, and damping agents. Agents within each category adopt the same strategy. We consider the problem of minimizing the maximum real part of the overall system eigenvalues.
- In the case of a line (platoon) of agents, we provide the optimal solution in closed form.
- In the case of a generic graph, under the assumption that all agents perform a damping action, we show that the optimization problem admits a global (though not necessarily isolated) minimum. We characterize such a minimum.
- We discuss how to select, among the equivalent minima, a solution that ensures robustness against variations in network topology.
- We discuss how to redesign the protocol, relying on simple gain-scaling, to account for acceleration bounds.

The theoretical analysis is complemented by simulations as well as real-world experiments conducted with a quadrotor swarm in a controlled indoor arena. The empirical results demonstrate that the proposed protocol successfully maintains formation integrity under dynamic conditions and validates the predicted benefits of damping agents.

2. Problem formulation

We consider a network of N agents with second-order dynamics:

$$\ddot{r}_i(t) = u_i(t), \;\; i = 1, 2, \dots, N, \tag{1}$$

where $r_i \in \mathbb{R}^d$ denotes the position of agent i, with respect to a common reference frame, in one, two, or three spatial dimensions, i.e., $d \in \{1, 2, 3\}$. This framework captures 1D platoons, 2D planar formations, and 3D spatial formations. The agents are categorized as follows:

- *Leader*: a designated agent that follows a prescribed reference position $\bar{r}$;
- *Regular agents*: agents that maintain the formation pattern based on local relative information;
- *Damping agents*: a subset of agents that additionally contribute to the damping of formation oscillations.

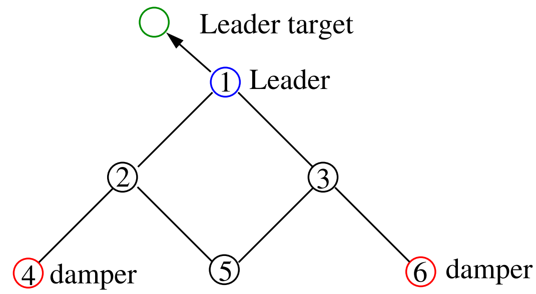

Fig. 1. Example of a formation graph. Node 1 is the leader, node 4 and 6 act as damping agents.

The inter-agent communication is modeled by an undirected graph $\mathcal{G} = (\mathcal{V}, \mathcal{E})$, where each node represents an agent. Two agents i and j can exchange information if and only if there exists an edge$(i, j) \in \mathcal{E}$. The set of neighbors of node i is denoted by Adj(i).

The control input $u_i(t)$ depends on the role of the agent. Following earlier work in platooning [8,19,20], the proposed control laws are:

- Leader (agent 1 in Fig. 1)

$$\begin{aligned}\ddot{r}_1(t) &= -\kappa(r_1(t) - \bar{r}) - \kappa \sum_{j \in \mathrm{Adj}(1)} (r_1(t) - r_j(t) - \bar{r}_{1j}) \\ &\quad - h\frac{d}{dt}(r_1(t) - \bar{r}) - h \sum_{j \in \mathrm{Adj}(1)} (\dot{r}_1(t) - \dot{r}_j(t));\end{aligned} \tag{2}$$

- Regular agent

$$\begin{aligned}\ddot{r}_i(t) &= -\kappa \sum_{j \in \mathrm{Adj}(i)} (r_i(t) - r_j(t) - \bar{r}_{ij}) \\ &\quad -h \sum_{j \in \mathrm{Adj}(i)} (\dot{r}_i(t) - \dot{r}_j(t));\end{aligned} \tag{3}$$

- Damper agent

$$\begin{aligned}\ddot{r}_i(t) &= -\kappa \sum_{j \in \mathrm{Adj}(i)} (r_i(t) - r_j(t) - \bar{r}_{ij}) \\ &\quad -h \sum_{j \in \mathrm{Adj}(i)} (\dot{r}_i(t) - \dot{r}_j(t)) - g\dot{r}_i(t).\end{aligned} \tag{4}$$

Here κ is the inter-agents stiffness factor, h the inter-agents damping factor, g is the damping node friction. The vector $\bar{r}_{ij}$ is the desired relative displacement between agents i and j, with $\bar{r}_{ij} = -\bar{r}_{ji}$. The model can be interpreted as a system of unit masses connected by springs (with stiffness κ) and dampers (with damping h), with some nodes having additional local damping g. To ensure the feasibility of the desired formation, we make the following assumption.

Assumption 1. Given the leader's target (constant) position $\bar{r}$ there exist target positions $\bar{r}_2, \bar{r}_3, \dots, \bar{r}_N$ such that

$$\bar{r}_{ij} = \bar{r}_i - \bar{r}_j, \quad \forall i, j.$$

This guarantees internal consistency of the relative position constraints (for instance, if 4 agents are on the vertices of a square, the desired positions for two opposite nodes must be the diagonal). If this condition is violated, steady-state errors may occur.

At steady state, the desired conditions are

$$r_1 = \bar{r}, \quad r_i - r_j = \bar{r}_{ij}, \quad \dot{r}_j = 0, \; \forall i, j. \tag{5}$$

Let the deviation from the desired formation be:

$$q = r - \bar{r},$$

where r and $\bar{r} \in \mathbb{R}^{dN}$ are the stacked vectors of actual and desired position, respectively. This vector has dimension N, $2N$, or $3N$ depending on the considered spatial dimensions.

For the 1D case ($d = 1$), the system dynamics can be compactly expressed as:

$$\ddot{q}(t) = -[hL + gE]\dot{q} - \kappa L q, \tag{6}$$

where $L \in \mathbb{R}^{N\times N}$ is the grounded graph Laplacian matrix [21] such that

$$L_{ij} = \begin{cases} 0 & \text{if} \quad \text{nodes } i \text{ and } j \text{ are not connected} \\ -1 & \text{if} \quad \text{nodes } i \text{ and } j \text{ are connected} \\ -\sum_{j\neq i} L_{ij} & \text{if} \quad i = j \neq 1 \\ -\sum_{j\neq i} L_{ij} + 1 & \text{if} \quad i = j = 1 \end{cases},$$

and $E \in \mathbb{R}^{N\times N}$ is a diagonal matrix with entries $E_{ii} = 1$ if agent i is a damper, 0 otherwise. The modification of L ensures the leader (node 1) is pinned to the external reference, making L nonsingular when the graph is connected [22–24].

Define the damping matrix:

$$H = hL + gE. \tag{7}$$

In higher dimensions ($d = 2, 3$), the dynamics decouple along each spatial axis, yielding d independent systems of the same form. Hence, theoretical analysis can focus on the scalar case without loss of generality.

The system can be written in state-space form as:

$$\dot{x}(t) = Ax(t), \quad A = \begin{bmatrix} 0 & I \\ -\kappa L & -(hL + gE) \end{bmatrix}, \tag{8}$$

where $x(t) = [q^\top(t) \ \ \dot{q}^\top(t)]^\top$.

We work under the following assumption.

Assumption 2. The stiffness coefficient $\kappa > 0$ is given; only the damping coefficients, h and g, have to be optimized.

Remark 2.1. The problem is ill-posed if κ is also a free variable, as the eigenvalues can be driven arbitrarily far into the left-half plane. As it is well known, this is unrealistic. We will discuss later on how one can determine a suitable κ.

We seek the fastest convergence to steady-state. Given a fixed stiffness coefficient $\kappa > 0$, the optimization problem can be stated as follows.

Problem 1. Given $\kappa > 0$, find $h \geq 0$, $g \geq 0$ that minimize the largest real part of the eigenvalues of the matrix A.

Claim 1. *Without loss of generality, and to simplify the analysis, we will assume $\kappa = 1$ in the sequel.*

This assumption is justified through a time rescaling argument $\tau\sqrt{\kappa} = t$ so that $dt = \sqrt{\kappa}d\tau$. Dividing (6) by κ we have that

$$\frac{1}{\kappa}\frac{d^2}{d\tau^2} = \frac{d^2}{dt^2}, \quad \frac{1}{\sqrt{\kappa}}\frac{d}{d\tau} = \frac{d}{dt}.$$

So if we find the optimal g^*, h^* corresponding to $\kappa = 1$ the resulting system is

$$\frac{d^2}{dt^2}q = -Lq - \left[h^* L \ - g^* E\right]\frac{d}{dt}q.$$

Scaling time

$$\frac{1}{\kappa}\frac{d^2}{d\tau^2}q = -Lq - \sqrt{\kappa}\left[h^* L \ - g^* E\right]\frac{1}{\kappa}\frac{d}{d\tau}q,$$

which writes as

$$\frac{d^2}{d\tau^2}q = -\kappa Lq - [hL + gE]\frac{d}{d\tau}q,$$

with $h = h^*\sqrt{\kappa}$ and $g = g^*\sqrt{\kappa}$. Since a rescaling of time does not affect the optimization problem, the following proposition holds.

Proposition 1. *If g^* and h^* are the optimal for $\kappa = 1$, then $g = g^*\sqrt{\kappa}$ and $h = h^*\sqrt{\kappa}$ are the optimal for a generic $\kappa > 0$.*

2.1. Lyapunov analysis

As discussed earlier, if parameters κ, h, and g are treated as free, it becomes possible to achieve arbitrarily fast—yet physically unrealistic—convergence. To avoid this, Problem 1 assumes κ is fixed, and focuses on optimizing h and g to improve the convergence rate. In this section, we propose a method to preliminarily choose a suitable value for κ, based on a constraint on the deviation from the desired formation.

We penalize deviation from the target configuration, both for the leader and for the relative agent positions. Consider the following quadratic cost:

$$J = \sum_{i\neq j} -L_{ij}\|(r_i - \bar{r}_i) - (r_j - \bar{r}_j)\|^2 + \|r_1 - \bar{r}_1\|^2 = \sum_{i\neq j} -L_{ij}\|q_i - q_j\|^2 + \|q_1\|^2 = q^\top Lq.$$

This cost penalizes relative deviations from the target distances between neighboring agents and the absolute deviation of the leader from its goal. Given a tolerance $\mu > 0$, we impose the constraint:

$$q(t) \in \mathcal{Q}_\mu = \{q : q^\top Lq \leq \mu\}. \tag{9}$$

This constraint ensures that the formation remains sufficiently close to the desired configuration during the evolution.

The following Proposition shows that the previous constraint remains satisfied during the whole transient starting from the rest condition.

Proposition 2. *Let $\mu > 0$ and desired positions $\bar{r}_i$ be given. Assume that (9) is satisfied at time $t = 0$. Assume that the initial velocities $\dot{r}_i(0) = \dot{q}(0) = 0$. Then the constraint (9) holds for all $t > 0$.*

Proof. Consider the Lyapunov function

$$V(q, \dot{q}) = \frac{1}{2}\dot{q}^\top\dot{q} + \frac{1}{2}q^\top\kappa Lq. \tag{10}$$

Taking the time derivative and substituting the system dynamics (6), we get:

$$\frac{d}{dt}\left[\frac{1}{2}\dot{q}^\top\dot{q} + \frac{1}{2}q^\top\kappa Lq\right] = \dot{q}^\top\ddot{q} + \dot{q}^\top\kappa Lq = -\dot{q}^\top[hL + gE]\dot{q},$$

which is negative semi-definite. Therefore, V is non-increasing over time. Since $\dot{q}(0) = 0$ by assumption, we have

$$\frac{\kappa}{2}q^\top(t)Lq(t) \leq \frac{\kappa}{2}q^\top(t)Lq(t) + \dot{q}^\top(t)\dot{q}(t) \leq \frac{\kappa}{2}q^\top(0)Lq(0) + \dot{q}^\top(0)\dot{q}(0) = \frac{\kappa}{2}q^\top(0)Lq(0) \leq \frac{\kappa\mu}{2}.$$

Then $\kappa q^\top(t)Lq(t)/2 \leq \kappa\mu/2$, dividing by $\kappa/2$, the proof is complete. □

Example 2.1. Consider $N = 3$ agents with desired positions $(0, 0)$, $(0, 1)$, $(1, 0)$, and assume a fully connected graph. Let the initial positions be $(1, 1)$, $(1, 2)$, $(2, 1)$, so that initially all agents are offset by the same vector $(1, 1)$. Thus, $q_i(0) = (1, 1)$ for all i, and the initial cost is $J = \sqrt{2}$. Thus, the formation deviation remains bounded by $\sqrt{2}$ throughout the transient.

If the damping matrix H is positive definite, then the Lyapunov function V also guarantees asymptotic stability, as established below.

Proposition 3. *Since the leader is pinned, the grounded Laplacian, L is positive definite and $\kappa, h > 0$, then $V \to 0$ as $t \to \infty$.*

Proof. This is a direct application of LaSalle's Invariance Principle. Since $\dot{V}(q, \dot{q}) \leq 0$, all trajectories converge to the largest invariant set contained in $\{(q, \dot{q}) \in \mathbb{R}^{2N} : \dot{V} = 0\}$. Since L is positive definite, the matrix H is also positive definite; therefore, the condition $\dot{V} = 0$ implies $\dot{q} = 0$, i.e., the set of zero velocity. In such a set, we have

$$\ddot{q} = -\kappa Lq.$$

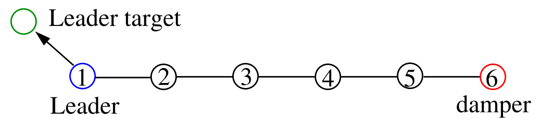

Fig. 2. The line graph. Node 1 is the leader, the final node 6 has a damping role.

If $q \neq 0$, then $\ddot{q} = d/dt[\dot{q}] \neq 0$, hence $\dot{q}$ cannot remain zero, contradicting invariance. Therefore, the only invariant set is the origin. □

Remark 2.2. The parameters κ, h, and g are assumed to be broadcast to the agents, which then implement the corresponding local control protocol.

3. Optimal solution for the line graph

The line graph with a designated leader (see Fig. 2) is a key special case in formation control, particularly in the context of vehicle platooning (see e.g., [25–31]).

In this section, we provide a closed-form optimal solution to Problem 1 for this topology.

Theorem 3.1. *Let $\kappa > 0$ be fixed. For a line graph topology with the leader at one end and a damping agent at the opposite end, the solution to Problem 1 is:*

$$h = g = \sqrt{\kappa}.$$

Proof. As mentioned before, we assume $\kappa = 1$, and we prove that the optimal parameters are $h = g = 1$ (then, the claim follows by Proposition 1). The proof proceeds in two steps. The first is to show that for $\kappa = 1$ and for $h = g = 1$, all $2N$ eigenvalues are at -1. The second is to show that if there exists an eigenvalue with real part less than -1, there must be another with real part greater than -1.

First part: All eigenvalues equal to -1 for $h = g = 1$. Recall from earlier that the eigenvalues of the system matrix correspond to the roots of the characteristic polynomial:

$$\Psi(s, h, g) = \det\left[s^2 I + (hL + gE)s + \kappa L\right] = 0. \tag{11}$$

Set $\kappa = h = g = 1$. The matrix becomes the following tridiagonal matrix.

$$M =$$

$$\begin{bmatrix} (s+1)^2+1 & -(s-1) & 0 & \dots & 0 \\ -(s+1) & (s+1)^2+1 & -(s-1) & \dots & 0 \\ 0 & -(s+1) & (s+1)^2+1 & \dots & 0 \\ \vdots & \vdots & \ddots & \ddots & \vdots \\ 0 & 0 & -(s-1) & (s+1)^2+1 & -(s-1) \\ 0 & 0 & 0 & -(s-1) & (s+1)^2 \end{bmatrix}.$$

It can be factored as:

$$M = \begin{bmatrix} (s+1) & -1 & 0 & \dots & 0 \\ 0 & (s+1) & -1 & \dots & 0 \\ 0 & 0 & (s+1) & \dots & 0 \\ \vdots & \vdots & \ddots & \ddots & 0 \\ 0 & 0 & 0 & (s+1) & -1 \\ 0 & 0 & 0 & 0 & (s+1) \end{bmatrix}$$

$$\times \begin{bmatrix} (s+1) & 0 & 0 & \dots & 0 \\ -1 & (s+1) & 0 & \dots & 0 \\ 0 & -1 & (s+1) & \dots & 0 \\ \vdots & \vdots & \ddots & \ddots & 0 \\ 0 & 0 & 0 & (s+1) & 0 \\ 0 & 0 & 0 & -1 & (s+1) \end{bmatrix}.$$

Therefore we have

$$\Psi(s) = (s+1)^N \ (s+1)^N.$$

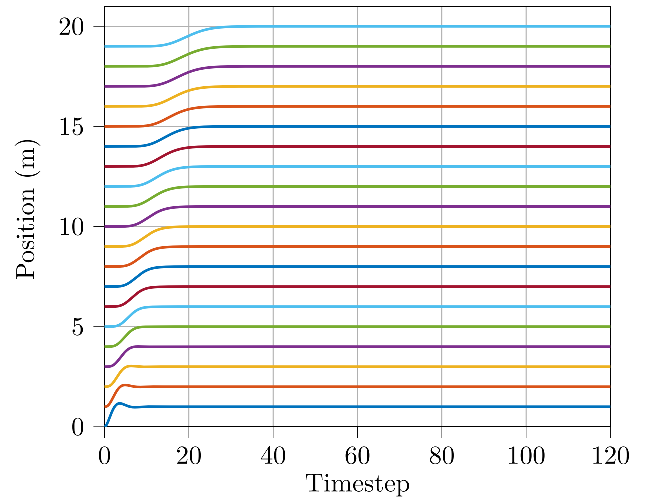

Fig. 3. The transient with 20 nodes. It is apparent that there is no reflection in the "wave" with $\kappa = h = g = 1$.

Hence, the only root is $s = -1$ of multiplicity $2N$, so all eigenvalues satisfy:

$$\max \ \Re(\sigma_k) = -1.$$

Second part: Any improvement on -1 leads to a worse eigenvalue elsewhere. Consider the polynomial again in (11). The constant term is $\Psi(0) = \det(\kappa L)$.Adopting the previous factorization, we have

$$\Psi(0) = \det(\kappa L) = \det \begin{bmatrix} 2 & -1 & 0 & \dots & 0 \\ -1 & 2 & -1 & \dots & 0 \\ 0 & -1 & 2 & -1 \dots & 0 \\ \vdots & \vdots & \ddots & \ddots & \vdots \\ 0 & 0 & -1 & 2 & -1 \\ 0 & 0 & 0 & -1 & 1 \end{bmatrix}$$

$$= \det \begin{bmatrix} 1 & -1 & 0 & \dots & 0 \\ 0 & 1 & -1 & \dots & 0 \\ 0 & 0 & 1 & \dots & 0 \\ \vdots & \vdots & \ddots & \ddots & 0 \\ 0 & 0 & 0 & 1 & -1 \\ 0 & 0 & 0 & 0 & 1 \end{bmatrix} \times \det \begin{bmatrix} 1 & 0 & 0 & \dots & 0 \\ -1 & 1 & 0 & \dots & 0 \\ 0 & -1 & 1 & \dots & 0 \\ \vdots & \vdots & \ddots & \ddots & 0 \\ 0 & 0 & 0 & 1 & 0 \\ 0 & 0 & 0 & -1 & 1 \end{bmatrix} = 1,$$

which is the product of all eigenvalues: $\prod_k \sigma_k = 1$. Since the modulus of the product is 1, if any eigenvalue has a real part < -1, then its modulus is > 1. To preserve the product, another eigenvalue must have the modulus < 1, implying a real part > -1. Therefore, it is not possible to improve the convergence rate beyond -1 without worsening another mode. Thus, the optimal solution is uniquely achieved for $h = g = 1$, completing the proof. □

Remark 3.1. This result is analogous to impedance matching in transmission line theory. For a mechanical analog of a transmission line with unit mass per unit length and stiffness κ, the characteristic impedance is $\sqrt{\kappa}$. Terminating the line with this value prevents wave reflections. In our case, setting the damper gain at the end of the formation to $g = \sqrt{\kappa}$ cancels reflections induced by the leader's motion. This is clearly illustrated in the simulation in Fig. 3. If we remove the "matching" term, setting $g = 0$, we get undesirable oscillations, as expected, due to wave reflection as shown in Fig. 4. The simulation shows that the transient is not over even if we triplicate the horizon $T = 120$.

The next corollary states that the damping matrix $(hL+gE)$ achieves the best damping among all the possible positive semi-definite damping matrices H.

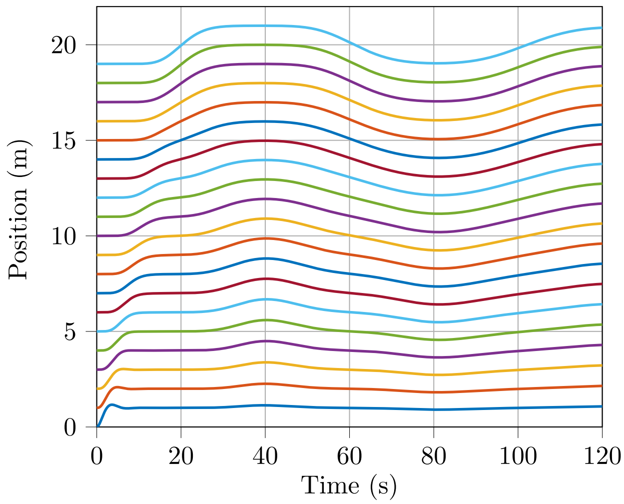

Fig. 4. The transient with 20 nodes without final impedance matching on a longer horizon $T = 120$. The reflection in the "wave" with $\kappa = h = 1$ but $g = 0$ causes quite undesirable oscillations.

Corollary 3.1. *Let $\kappa > 0$ be fixed and consider the eigenvalue optimization*

$$\min_{H \geq 0} \max_{k} \Re(\sigma_k),$$

where

$$\Psi(s,\kappa,H) = \det\left[s^2 I + Hs + \kappa L\right] = 0. \tag{12}$$

Then the optimal damping matrix is

$$H = (hL + gE),$$

with $h = g = \sqrt{\kappa}$

Proof. We already showed that for this choice, all eigenvalues are located at $-\sqrt{\kappa}$. Since the product of eigenvalues equals $\Psi(0,\kappa,H) = \det(\kappa L) = \kappa^N$, no configuration can place all eigenvalues further left on the complex plane without violating the constraint on the determinant (product of roots). Hence, this choice minimizes the spectral abscissa. □

4. The case of a generic graph

We now consider the scenario where the damping matrix is of a generic form, and H and E are not restricted to line graphs. The eigenvalues of the system are the roots of the polynomial:

$$\Psi(s,\kappa,h,g) = \det\left[s^2 I + (hL + gE)s + \kappa L\right] = 0. \tag{13}$$

We begin by providing the following important lower bound for the optimal solution.

Proposition 4. *Let (h^*, g^*) be the optimal parameters. Then the maximum real part of the eigenvalues satisfies:*

$$\max_i \Re(\sigma_i) \geq -\sqrt[2N]{\kappa \det(L)}.$$

The proof follows the same reasoning as the corollary for the line-graph case and relies on the fact that the determinant of a matrix equals the product of its eigenvalues.

We now consider the case $E = I$, corresponding to the situation where each agent acts as a damper. In this setting, the damping matrix is modeled as a linear combination of L and the identity matrix.

The following theorem establishes the quasi-convexity of the optimization problem.

Theorem 4.1. *Let $E = I$. For fixed κ, the sublevel sets of the maximum real part function*

$$Sub(g,h) = \{(g,h) : \max_i \Re(\sigma_i) \leq -\xi\},$$

with $\xi > 0$ a parameter, are convex polygons. That is, the function $\max_i \Re(\sigma_i)$ is quasi-convex.[1]

Precisely such sub-level sets are the intersection of stripes defined by the inequalities

$$2\xi \leq h\lambda_i + g \leq \max\left\{2\sqrt{\lambda_i}, \xi + \frac{\lambda_i}{\xi}\right\} \quad i = 1,2,\dots,N. \tag{14}$$

Proof. Assume $\kappa = 1$. Let $Q^\top L Q = \Lambda = \mathrm{diag}\{\lambda_1, \lambda_2, \dots\}$ be the diagonalization of L. Then (13) becomes:

$$\Psi(s,k,h,g) = \det\left[s^2 I + (h\Lambda + gI)s + \Lambda\right] = 0. \tag{15}$$

The eigenvalues are the roots of the equations:

$$s^2 + (h\lambda_i + g)s + \lambda_i = 0, \quad i = 1,2,\dots,N, \tag{16}$$

whose maximum real part is

$$\frac{-(h\lambda_i + g) + \sqrt{\left[(h\lambda_i + g)^2 - 4\lambda_i\right]^+}}{2} \leq -\xi \; i = 1,2,\dots,N,$$

where we denote by $[x]^+$ the function $[x]^+ = \max\{x, 0\}$. The proof follows by noticing that the set

$$\mathcal{I} = \{x : \frac{-x + \sqrt{[x^2 - 4\lambda_i]^+}}{2} \leq -\xi\} \tag{17}$$

is an interval $[a_i, b_i]$ for $x = (h\lambda_i + g)$ for suitable a_i and b_i, so the polygon is defined by the inequalities $a_i \leq h\lambda_i + g \leq b_i$. To prove that $\mathcal{I}$ is an interval, consider the set of points that satisfy the inequality in (17), which can be written as

$$\sqrt{[x^2 - 4\lambda_i]^+} \leq x - 2\xi.$$

Clearly, we must have

$$x \geq 2\xi \tag{18}$$

(hence x must be positive). Then square both sides to obtain

$$[x^2 - 4\lambda_i]^+ \leq x^2 + 4\xi^2 - 4\xi x.$$

If $x^2 \leq 4\lambda_i$, and since x is positive, we have

$$x \leq 2\sqrt{\lambda_i}. \tag{19}$$

Therefore, the inequality is true. Conversely let $x^2 > 4\lambda_i$, namely $x > 2\sqrt{\lambda_i}$, we have $[x^2 - 4\lambda_i]^+ = x^2 - 4\lambda_i$ and therefore, by eliminating x^2, we get $-4\lambda_i \leq 4\xi^2 - 4\xi x$ or

$$x \leq \xi + \frac{\lambda_i}{\xi}. \tag{20}$$

The overall set results by considering that it must be $x \geq 2\xi$ and that either (19) or (20) must be true (so x cannot exceed the larger between $2\sqrt{\lambda_i}$ and $\xi + \lambda_i/\xi$). Letting $x = h\lambda_i + g$ for all i, we have that the set is defined by the inequalities in (14). □

Corollary 4.1. *Under the same assumptions of the theorem, any local minimum is a global minimum.*

Proof. This is a standard property of the quasi-convex functions. □

The following theorem provides a possible optimal value (non-unique in general) for h and g.

[1] A function is quasi-convex if and only if its sublevel sets are convex. For instance, $\sqrt{|x|}$ is not convex, but quasi-convex.

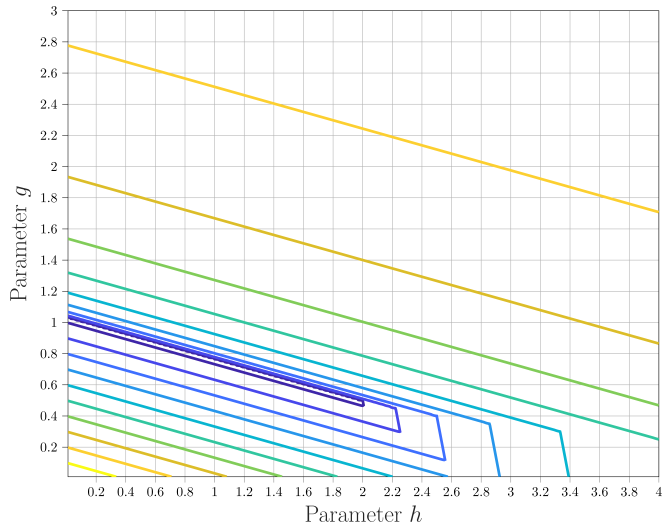

Fig. 5. The sublevel set of the function $\max_i \Re(\sigma_i)$.

Theorem 4.2. *Let $E = I$ and fix κ. Then an optimal choice is:*

$$(g^*, h^*) = (2\sqrt{\kappa\lambda_1}, 0), \tag{21}$$

where λ_1 is the smallest eigenvalue of L. The corresponding optimal value for the maximum real part of the eigenvalues is $-\sqrt{\lambda_1\kappa}$.

Proof. Assume $\kappa = 1$. Consider first of the Eqs. (16) for $i = 1$

$$s^2 + (h\lambda_1 + g)s + \lambda_1 = 0. \tag{22}$$

Its roots have product $\sigma_1\sigma_2 = \lambda_1$, hence their real parts cannot be both smaller than $-\sqrt{\lambda_1}$. This number is a lower bound for the optimum. Take $g = 2\sqrt{\lambda_1}$ and $h = 0$. Then the two roots are real negative and both equal to $-\sqrt{\lambda_1}$. We prove that all the other roots for $i > 1$ have real part exactly equal to $-\sqrt{\lambda_1}$. For $i > 1$ the equation is

$$s^2 + 2\sqrt{\lambda_1}s + \lambda_i = 0,$$

and the corresponding root pair is complex

$$\frac{-2\sqrt{\lambda_1} + \sqrt{4\lambda_1 - 4\lambda_i}}{2} = -\sqrt{\lambda_1} \pm j\sqrt{\lambda_i - \lambda_1},$$

with real part $-\sqrt{\lambda_1}$. □

In Fig. 5, we plot the sublevel sets for the case $\kappa = 1$ and

$$L = \begin{bmatrix} 3 & -1 & -1 & 0 & 0 \\ -1 & 3 & 0 & -1 & 0 \\ -1 & 0 & 3 & -1 & -1 \\ 0 & -1 & -1 & 3 & -1 \\ 0 & 0 & -1 & -1 & 2 \end{bmatrix}.$$

The optimal parameters are approximately $g = 0.77$, $h = 0.99$, and the dominant eigenvalue is $\max_i \Re(\sigma_i) = -0.5176$. Note that the minimum is not isolated.

Remark 4.1. The solution (21) provides one possible optimal choice of the parameters in terms of the spectral abscissa. However, the optimal solution is not unique, and other pairs (g, h) yield the same dominant eigenvalue.

It is important to note that the optimal value $h^* = 0$, although theoretically optimal for the convergence rate, removes the relative velocity coupling between neighboring agents. In practice, this coupling plays an important role in improving robustness and attenuating disturbances.

For this reason, it is often preferable to select a different optimal pair that retains a non-zero relative damping term. In particular, a convenient choice is to minimize the value of g, which reduces the absolute viscous force that may deform the formation when the leader moves with non-zero velocity.

In view of the above remark, we wish to characterize the set of all minimizers, which turns out to be a segment. Let $\kappa = 1$, consider expression (14) and let us notice that the minimum $-\xi$, namely the maximum ξ, is the largest possible value such that all the stripes in (14) are non-empty

$$\max \xi \ : \ 2\xi \le \max\left\{2\sqrt{\lambda_i}, \xi + \frac{\lambda_i}{\xi}\right\} \ \ i = 1, 2, \dots, N. \tag{23}$$

The ith inequality is true if either $2\xi \le 2\sqrt{\lambda_i}$ or $2\xi \le \xi + \frac{\lambda_i}{\xi}$ is true, namely

$$\xi \le \sqrt{\lambda_i} \text{ or } \xi^2 \le \lambda_i,$$

that are the same condition, meaning that the optimal is $\xi^* = \sqrt{\lambda_1}$. Correspondingly, the strip associated with the first inequality in (14) becomes the line

$$h\lambda_1 + g = 2\xi^* = 2\sqrt{\lambda_1}. \tag{24}$$

Therefore, the set of optimal solutions is the segment defined by (24), subject to all the other inequalities in (14), excluding the first that is collapsed to a line. In Fig. 5, one can see this segment where the level surfaces meet the optimal value.

An important issue is how one can choose a value on the optimal line (24). A good criterion, which is in contrast to the theoretically motivated (21), is to take on the segment (24) the point that minimizes g^* and (as it is immediate) maximizes h^*. By reducing g^*, we minimize an absolute viscous force, which is important for damping but can introduce a deformation when the leader speed is non-zero. We also show that this choice increases robustness. We will come back to this later on.

The next corollary shows that, for fixed κ, the worst topology is the line, in agreement with existing literature [22–24].

Corollary 4.2. *Let L_{line} be the Laplacian of the line graph with N nodes and smallest eigenvalue λ_1^{line}. Then for any other connected topology with Laplacian L and smallest eigenvalue λ_1, the optimal eigenvalue satisfies:*

$$\sqrt{\kappa\lambda_1} \ge \sqrt{\kappa\lambda_1^{line}}.$$

Proof. Any connected graph contains a spanning line graph (a path crossing all N nodes), so we can construct $L_{\text{line}} < L$ (in the sense that $L - L_{\text{line}}$ is positive semi-definite). This implies $\lambda_1^{\text{line}} \le \lambda_1$, and hence the optimal damping performance (in terms of real parts of eigenvalues) is always worse in the line topology. □

4.1. Choosing κ: convergence speed and actuator exploitation

So far, we have considered a fixed $\kappa > 0$ and optimized the damping. The previous investigation provides a guideline for the choice. We have seen that the optimal maximum real part is $-\sqrt{\kappa\lambda_1} = -\sigma_1$. This is the dominant real part that provides a clue for the speed of convergence, which is imposed by the dominant eigenvalue, and then equivalent to $e^{-\sigma_1 t}$. The speed of convergence is associated with the actuator exploitation, and it should be decided accordingly. Once σ_1 is fixed, we consequently choose $\kappa = \sigma_1^2/\lambda_1$.

Furthermore, the system bandwidth is associated with its dominant eigenvalue $\omega_{bw} = 2\pi\sigma_1$, henceforth κ can be chosen by specifying a proper ω_{bw}^*.

A more rigorous possibility for choosing κ is based on the maximum acceleration $a_{\max}$. The idea is to solve the problem for $\kappa = 1$ (computing the optimal g^* and h^*) that corresponds to a maximum acceleration a_1

and subsequently scaling κ, according to the ratio $a_{\max}/a_1$ and updating g and h as follows (see Proposition 1):

$$\kappa = \frac{a_{\max}}{a_1}, \ g = g^* \sqrt{\kappa} \ h = h^* \sqrt{\kappa}. \tag{25}$$

The values of h and g in (25) are optimal for the new κ, as we have seen in Proposition 1.

We can consider a set of candidate initial positions $q(0) \in \mathcal{Q}$ (possibly a singleton) and $\dot{q}(0) = 0$ and compute the maximum acceleration a_1 for all possible initial conditions in this set. Specifically, consider a single nominal initial condition $q(0) = q_0$, $\dot{q}(0) = 0$. Assuming $k = 1$, the control variable $u(t)$ over time is described by the impulse response of the linear system with matrices

$$A = \begin{bmatrix} 0 & I \\ -L & -(h^*L + g^*E) \end{bmatrix} \ B = \begin{bmatrix} q_o \\ 0 \end{bmatrix} \ C = \begin{bmatrix} -L & -(h^*L + g^*E) \end{bmatrix}.$$

Adopting standard software, we can straightforwardly compute the impulse response and its maximum value. Choosing a different $\kappa \neq 1$, in view of (25), results in the κ–system

$$A_\kappa = \begin{bmatrix} 0 & I \\ -\kappa L & -\sqrt{\kappa}(h^*L + g^*E) \end{bmatrix} \ C_\kappa = \begin{bmatrix} -\kappa L & -\sqrt{\kappa}(h^*L + g^*E) \end{bmatrix},$$

with $B_\kappa = B$. The transfer functions of the two systems are related by

$$C_\kappa[sI - A_\kappa]^{-1}B_\kappa = \kappa C[sI - \sqrt{\kappa}A]^{-1}B.$$

To prove this, apply the state transformation (that of course leaves unchanged the transfer function)

$$\hat{A}_\kappa = \begin{bmatrix} I & 0 \\ 0 & \frac{1}{\sqrt{\kappa}}I \end{bmatrix} \begin{bmatrix} 0 & I \\ -\kappa L & -\sqrt{\kappa}(h^*L + g^*E) \end{bmatrix} \begin{bmatrix} I & 0 \\ 0 & \sqrt{\kappa}I \end{bmatrix} = \sqrt{\kappa}A,$$

$$\hat{C}_\kappa = \begin{bmatrix} -\kappa L & -\sqrt{\kappa}(h^*L + g^*E) \end{bmatrix} \begin{bmatrix} I & 0 \\ 0 & \sqrt{\kappa}I \end{bmatrix} = \kappa C,$$

$$\hat{B}_\kappa = \begin{bmatrix} I & 0 \\ 0 & \frac{1}{\sqrt{\kappa}}I \end{bmatrix} B_\kappa = B.$$

The impulse response of the κ–systems is

$$C_\kappa e^{A_\kappa \tau} B_\kappa = \kappa C e^{\sqrt{\kappa}A\tau} B = \kappa C e^{At} B, \tag{26}$$

where we adopted the scaled time $t = \sqrt{\kappa}\tau$. Since scaling time does not change the maximum, the only variation is due to the amplitude scaling of a factor κ. Hence, given the maximum admissible norm for the acceleration, $a_{\max}$, we can take κ as in (25) with

$$a_1 = \max_{t \geq 0} \|Ce^{At}B\|.$$

Remark 4.2. If the set of all possible initial conditions is a polytope $\mathcal{Q}$, then the overall maximum is achieved at some vertex of $\mathcal{Q}$. Consequently, it suffices to compute the maximum over all vertices.

5. Robustness of the protocol and decentralization

An optimal pair of parameters (g, h), designed for a specific graph topology with Laplacian L and damping matrix H, may become non-optimal if the topology changes. However, stability is not compromised, as the following proposition shows.

Proposition 5. *System (6) is asymptotically stable for all positive values of κ, h, and g as long as the graph is connected.*

Proof. It follows from the proof of Theorem 4.1. The system eigenvalues are the roots of the polynomials in (16), hence all the roots have a negative real part. □

The previous proposition guarantees robustness to changes in topology, but it does not address the case where the topology is time-varying.

If the communication topology changes arbitrarily fast, stability can be lost. However, stability is preserved if changes occur with sufficient dwell time. Let us define:

$$T^* \doteq \min\{T : \ \|e^{A_k\sigma}\| \leq 1 - \epsilon, \ \forall \sigma > T, \forall k\} \tag{27}$$

for a given family of Hurwitz matrices A_k and tolerance $\epsilon > 0$. Then we have the following.

Proposition 6 ([32]). *Let A_k, $k = 1, \dots, N$, be a family of Hurwitz matrices. Consider the switched system:*

$$\dot{x}(t) = A(t)x(t), \ A(t) = A_k, \ t_k \leq t \leq t_{k+1}. \tag{28}$$

If the switching instants t_k satisfy a dwell time condition $t_{k+1} - t_k \geq T > T^*$, then the system is asymptotically stable.

Remark 5.1. The value T^* can be computed numerically by plotting the function $\phi(\sigma) = |e^{A_k\sigma}|$ and identifying the smallest σ for which all trajectories decay below $1 - \epsilon$.

This result ensures that stability is preserved under slow enough switching.

Let us now consider the performance loss due to communication loss. Suppose that some communication links fail, resulting in a degraded Laplacian L_k. We assume a nominal design based on a fixed Laplacian L and optimal parameters (κ, h, g), and we ask: *how much does performance degrade under link loss?*

Let the damping matrix remain $E = I$, and $\kappa = 1$ fixed. The following theorem provides a performance bound based on the minimum algebraic connectivity across all possible topologies.

Theorem 5.1. *Let L_k, $k = 1, 2 \dots, N$ be a set of possible Laplacians (one for each failed-link configuration), and let $\lambda_{\min}$ be the smallest of the smallest eigenvalues of all possible L_k. Let $-r^*$ denote the largest real part of the roots of the second-order polynomial:*

$$s^2 + (h\lambda + g)s + \lambda = 0 \tag{29}$$

evaluated at $\lambda = \lambda_{\min}$. Then the dominant eigenvalue σ of the system for any L_k satisfies:

$$\Re(\sigma) \leq \max\left\{-r^*, -\frac{1}{h}\right\} = -\min\left\{r^*, \frac{1}{h}\right\}. \tag{30}$$

Proof. We consider the diagonalized system as in (15). Since the matrix is diagonal this corresponds to the Eq. (29). All possible closed-loop systems eigenvalues correspond to some $\lambda \geq \lambda_{\min}$ eigenvalue of the true configuration L_k.

The proof then requires showing that if $\lambda > \lambda_{\min}$, condition (30) holds. We prove this by proving that either $\sigma_1(\lambda) \leq -1/h$, or $\sigma_1(\lambda)$ is decreasing in λ. Assume $\Re[\sigma_1(\lambda)] > -1/h$. We distinguish two cases.

(I) $\sigma_1(\lambda)$ is complex (hence $\sigma_2(\lambda)$ is the conjugate). The real part is

$$\Re[\sigma_1(\lambda)] = -\frac{h\lambda + g}{2}.$$

This function is clearly decreasing in λ.

(II) $\sigma_1(\lambda)$ is real (hence $\sigma_2(\lambda) \leq \sigma_1(\lambda)$). We now compute the derivative of $\sigma_1(\lambda)$. Adopting the theorem of the derivative implicitly defined functions[2] we have:

$$\frac{ds}{d\lambda} = -\frac{sh + 1}{2s + h\lambda + g}, \tag{31}$$

where $s = \sigma_1$ is the larger real root that has the well-known form

$$\sigma_1 = -(h\lambda + g)/2 + \sqrt{\Delta}/2,$$

[2] If $f(x, y) = 0$, then $dy/dx = -[\partial f/\partial x]/[\partial f/\partial y]$.

with $\Delta = (h\lambda + g)^2 - 4\lambda > 0$. Replacing in (31) we get

$$\frac{ds}{d\lambda} = -\frac{sh+1}{\sqrt{\Delta}} < 0, \tag{32}$$

where the last inequality is due to the fact that the numerator of the fraction is positive because we are considering the case $s = \sigma_1(\lambda) > -1/h$. □

Remark 5.2. As anticipated in Remark 4.1, choosing $h = 0$, although equivalent from the optimization problem, could not be a good choice from the robustness standpoint. From (30) we see that if we take $h = 0$, then the limiting term $-1/h$ becomes $-\infty$, so the only bound remains $-r^*$. When the connectivity is low, λ_{min} is close to 0, and consequently $-r^*$ is also close to zero, making the bound rather weak.

5.1. Discussion about decentralization

As far as the real-time control is concerned, our protocol is fully decentralized. This is true as long as we fix a target with a final zero speed. Note that, since convergence speed is our concern, this makes sense since the speed of convergence is referred to an equilibrium.

This aspect has to be re-discussed if we admit that the leader can impose a moving reference. Assume that the leader imposes a constant speed $\bar{v}$. The reference becomes

$$\bar{r} = \bar{v}\, t$$

Then there are two options. The first is that the leader broadcasts, in real time, the desired speed $\bar{v}$. In this case, the protocol should be transformed by replacing the term $-g\dot{r}_k$ by

$$-g(\dot{r}_k - \bar{v}). \tag{33}$$

Then the theory works without change. All the agents reach their target position asymptotically, referred to a reference frame moving with speed $\bar{v}$.

The second case is that, conversely, the leader cannot broadcast the desired speed. In this new situation, the dissipation terms $-g\dot{r}_k$ create deformation of the formation geometry due to this viscosity force. For instance, in the platooning case, the steady-state distance between agents increases (decreases) if the leader is pulling (pushing). This effect is clearly limited if the parameter κ is large enough to ensure rigidity. In any case, convergence is not compromised.

To better analyze the moving formation case, it is convenient to consider the velocities. These converge to the desired value $\bar{v}$ (even with no broadcasting). Let the desired leader velocity be constant and equal to $\bar{v}$, and define the velocity error, $v_i = \dot{r}_i - \bar{v}$. Since $\bar{v}$ is constant, we have $\dot{v}_i = \ddot{r}_i$. Consider position Eqs. (2)–(4). Differentiating them yields the following dynamics for the velocity errors:

$$\ddot{v}(t) = -[hL + gE]\dot{v} - \kappa L v. \tag{34}$$

Therefore, the velocity errors evolve according to the same dynamics as the position deviations in (6). As a consequence, all the optimality results derived in the previous sections also apply to the convergence of the velocities to the desired value $\bar{v}$.

As far as the formation geometry is concerned, clearly, this is, in general, a centralized decision that has to be communicated to the agent. Moreover, the optimal values depend on the Laplacian of the connection, hence require a centralized decision. This information has to be established offline and communicated to the agents, including their role, i.e., regular/damping agent.

A notable exception is the platooning case. In a line topology the structure of the formation allows a simple decentralized implementation. The leader only needs to transmit the desired spacing and the parameter κ to its follower, which in turn relays this information to the next agent, and so on. The last agent in the chain naturally assumes the damping role, since it has no followers, thereby implementing the impedance-matching condition $h = g = \sqrt{\kappa}$.

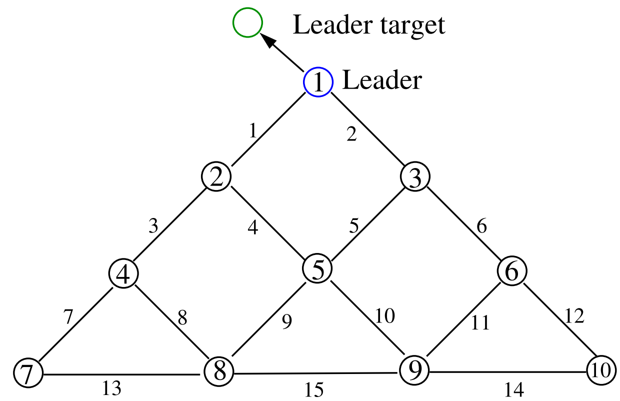

Fig. 6. The nominal topology of simulations.

More general formation geometries can also be spontaneously generated, given a pattern. If, for instance, the overall pattern is a triangle-like formation, or a V-like (bird flight) formation, such patterns can be easily re-configured when a new agent joins the group by just spontaneously occupying one of the last positions. In this case, each agent can well ignore its absolute position and just be aware of the desired position with respect to its neighbors. For spontaneously forming patterns, it is convenient to adopt the same interchangeable control values κ^*, g^*, h^*.

From the control implementation viewpoint, the proposed protocol is fully decentralized. Each agent uses only relative position and velocity measurements from its neighbors, together with its own velocity when acting as a damping node.

However, the parameters κ, h, and g depend on the topology through the Laplacian matrix. Consequently, their optimal values must be computed offline and broadcast to the agents together with their assigned role (regular or damping node).

6. Simulations

In this section, we present the simulation of a formation of 10 drones with the nominal communication topology shown in Fig. 6.

We have fixed $\kappa = 1$. For this setup, the level surfaces of the function we optimize are shown in Fig. 7. Possible optimal values for h and g turn out to be $h^* = 3.98$ and $g^* = 0.25$, corresponding to the dark blue segment in Fig. 7.

The step response of the formation under the nominal topology is shown in Fig. 8 (top).

We next consider the case where some communication links intermittently fail. Four distinct failure patterns are tested:

	Topology_1	Topology_2	Topology_3	Topology_4
Failed links	$\{2, 6, 8\}$	$\{4, 5, 13\}$	$\{1, 3, 7\}$	$\{2, 6, 12\}$

Each failure configuration persists for an interval of $T_{\text{fail}} = 3$ s, and the four patterns repeat periodically four times, yielding a total simulation horizon of $T = 48$ s. The corresponding step response for the switching topology is shown in Fig. 8 (bottom).

As expected, the loss of connectivity introduces irregularities in the transient response.

From the robustness perspective, as discussed in Remark 4.1 and Remark 5.2, the choice (21)—optimal for the nominal topology—may perform poorly, from the robustness point of view, when the topology changes. To illustrate this effect, we consider an alternative optimal pair $g^* = 0.500$ and $h^* = 0$ corresponding to one of the stationary points of (21). The resulting transient is reported in Fig. 9. Although the convergence rate remains nearly the same, noticeable oscillations arise due to the intermittent loss of connections.

As another experiment, we set $g = 0$, keeping $h = 0.39$, to see the effect of removing the absolute damping. The result is a considerable overshoot as shown in Fig. 10.

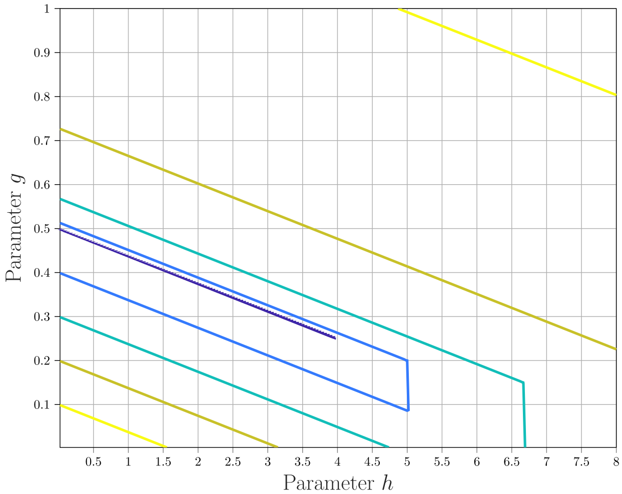

Fig. 7. The maximum real part as a function of h and g. We assume $\kappa = 1$. The optima are on the dark blue segment.

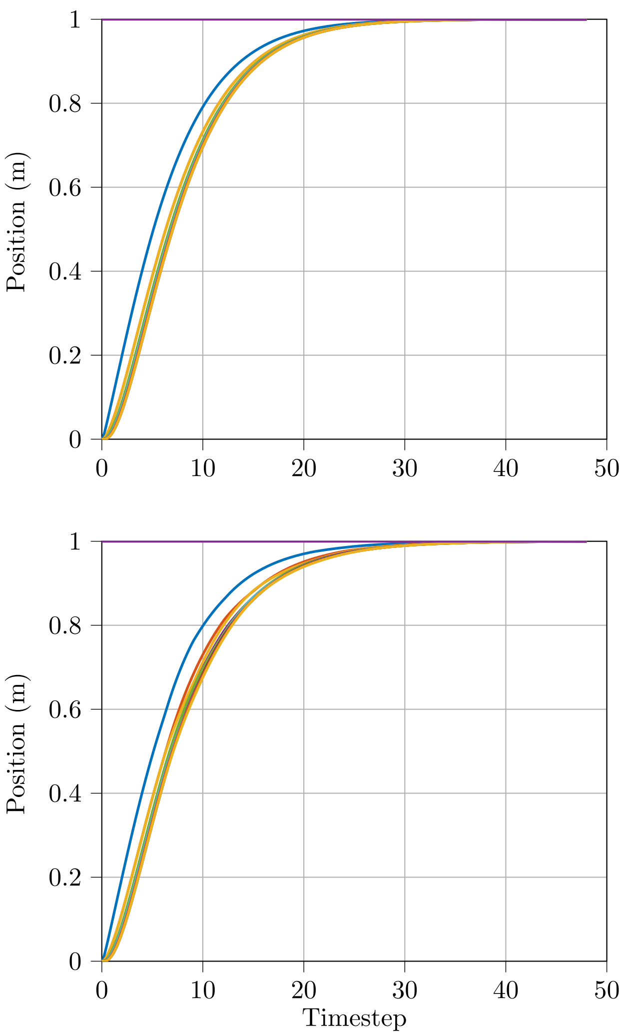

Fig. 8. The step response under nominal topology (top) and under the switching topology (bottom). We took, among the optimal pairs (g^*h^*), the value that minimizes the g^* component, namely $(g^*, h^*) = (0.25, 3.98)$. In this way, we ensure robustness.

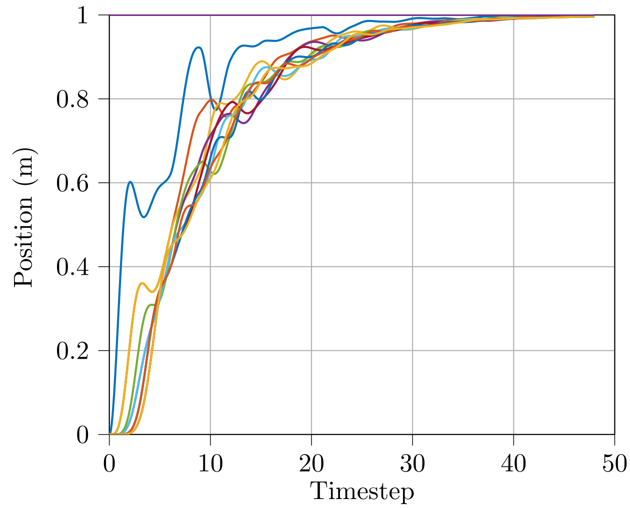

Fig. 9. The step response under a different optimal choice $(g^*, h^*) = (2\sqrt{\kappa\lambda_1}, 0)$. We observe that the convergence speed is essentially preserved, but oscillations appear due to a lack of robustness.

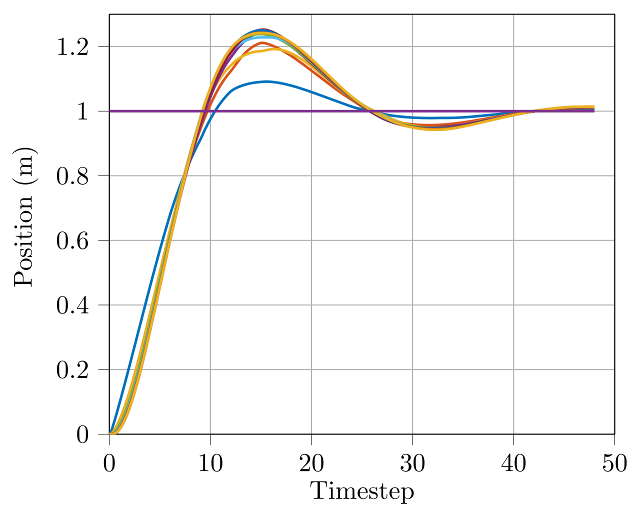

Fig. 10. The step response under the choice and switching topology $(g^*, h^*) = (0, 0.39)$. We observe that in this case, we have a considerable overshoot.

7. Experimental validation

To evaluate the performance and practical feasibility of the proposed formation control strategy with damping agents, we conducted a series of real-world experiments using a swarm of quadrotor Unmanned Aerial Vehicles (UAVs). The tests were carried out in the Drones Arena at the University of Trieste, a dedicated indoor flight facility equipped with a high-precision motion capture system and real-time tracking infrastructure developed by Ant-X.[3] This arena provides a controlled environment suitable for repeatable multi-agent flight tests, allowing to accurately measure position, velocity, and acceleration data in three dimensions.

The experimental setup involves a team of four quadrotors operating in a leader–follower configuration. One drone is designated as the leader, which receives target inputs and dynamically generates its trajectory through sequential target point calculation at each control step. The remaining three agents act as followers with no knowledge

[3] https://antx.it/educational-products-antx/dronelab-antx/

of the global target, relying exclusively on local relative measurements from neighboring agents to maintain formation. Among the followers, one is assigned the role of a damping agent, implementing an extended control strategy that incorporates absolute velocity feedback in addition to local relative measurements. This configuration is consistent with the theoretical model described in previous sections, and the experimental results qualitatively confirm the expected stability and convergence properties of the proposed control protocol.

The formation control parameters were set to $\kappa = 200$, $h = 14.14$, and $g = 14.14$, chosen based on the optimization procedure described in Section 5, specifically following the optimal solution $h = g = \sqrt{\kappa}$ for line graph topology.

The data was collected at a frequency of 10 Hz and includes 3D position and acceleration measurements. Time is in second, distance in meters.

The initial position for the drones are $x_1(0) = x_2(0) = x_3(0) = x_4(0) = 2$, $y_1(0) = 1$, $y_2(0) = 0$, $y_3(0) = -1$, $y_4(0) = -2$, $z_1(0) = z_2(0) = z_3(0) = z_4(0) = 0.5$. All initial velocities are set to 0. The reference trajectory for the leader is chosen to be piecewise-constant, and is the following:

$$\bar{x} = \begin{cases} -2, & t \in [0, 24) \\ 0, & t \in [24, 48) \\ 2, & t \geq 48 \end{cases}, \quad \bar{y} = \begin{cases} 1, & t \in [0, 24) \\ 2, & t \in [24, 48) \\ 1, & t \geq 48 \end{cases} \quad \bar{z} = 1, \ t \geq 0$$

The desired relative configuration is such that all drones share the same x and z coordinates, while maintaining a one-meter spacing in the y direction: $y_1 - y_2 = 1$, $y_2 - y_3 = 1$, and $y_3 - y_4 = 1$, which corresponds to the configuration at $t = 0$.

Position trajectories for all drones are shown in Fig. 11, confirming successful tracking of the Leader's trajectory across all axes. In the x and z directions, the formation remains tightly synchronized, while the y–component reflects the lateral offset due to the initial spacing, maintained consistently throughout the maneuver. These results indicate that relative positioning and local feedback are sufficient to enforce coherent group motion without centralized control.

To visualize the collective 3D evolution of the swarm, Fig. 12 shows the drone trajectories projected on the three principal planes: top view ($x - y$ plane) , side view ($x - z$ plane), and front view ($y - z$ plane). Circles denote the initial positions and squares the final ones. The initial configuration is the same as described above.

The coordinated motion is clearly evident, with agents maintaining consistent relative spacing throughout the maneuver. The Tail drone (green) shows visibly smoother transitions, especially in the lateral and vertical dimensions, consistent with the intended damping effect. The plotted start and end positions further confirm convergence and formation stability.

To quantitatively assess the preservation of the formation, inter-agent distances from the Leader to each follower were computed and are plotted in Fig. 13. The distances remain bounded across the experiment, exhibiting small and rapidly decaying transients in response to sudden changes in the leader's velocity. Notably, the distance to the Tail drone displays the lowest oscillatory behavior, which empirically supports the theoretical role of damping agents in suppressing disturbance propagation along the formation.

Overall, the empirical observations strongly align with the theoretical guarantees derived in earlier sections. The formation remains asymptotically stable under the distributed control protocol, even in the presence of external disturbances and dynamic trajectory changes. The inclusion of a damping agent significantly improves transient behavior, reducing both overshoot and acceleration spikes. These results underscore the feasibility and robustness of the proposed decentralized control strategy for real-world applications involving UAV swarms and multi-agent formations.

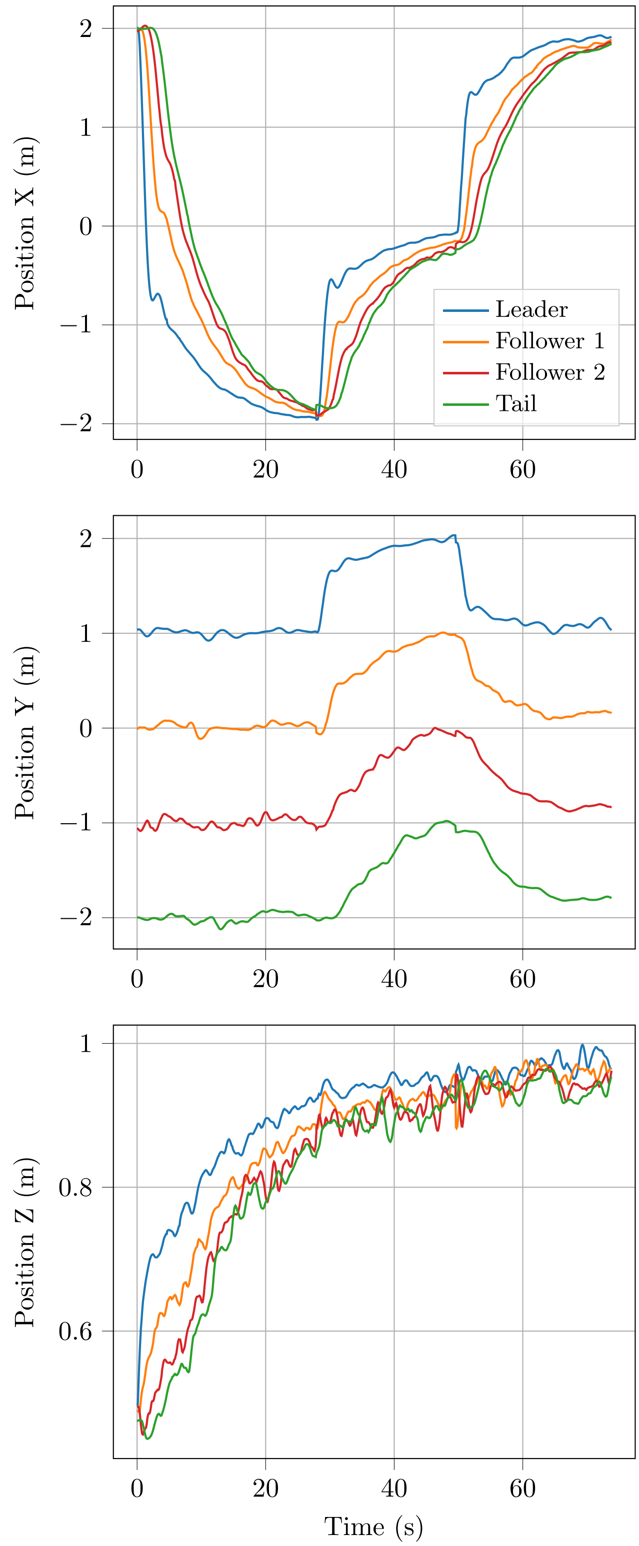

Fig. 11. Position trajectories for all drones tracking the Leader's trajectory across all axes. In the x and z directions, the formation remains tightly synchronized, while the y–component reflects the lateral offset due to the initial spacing, maintained consistently throughout the maneuver.

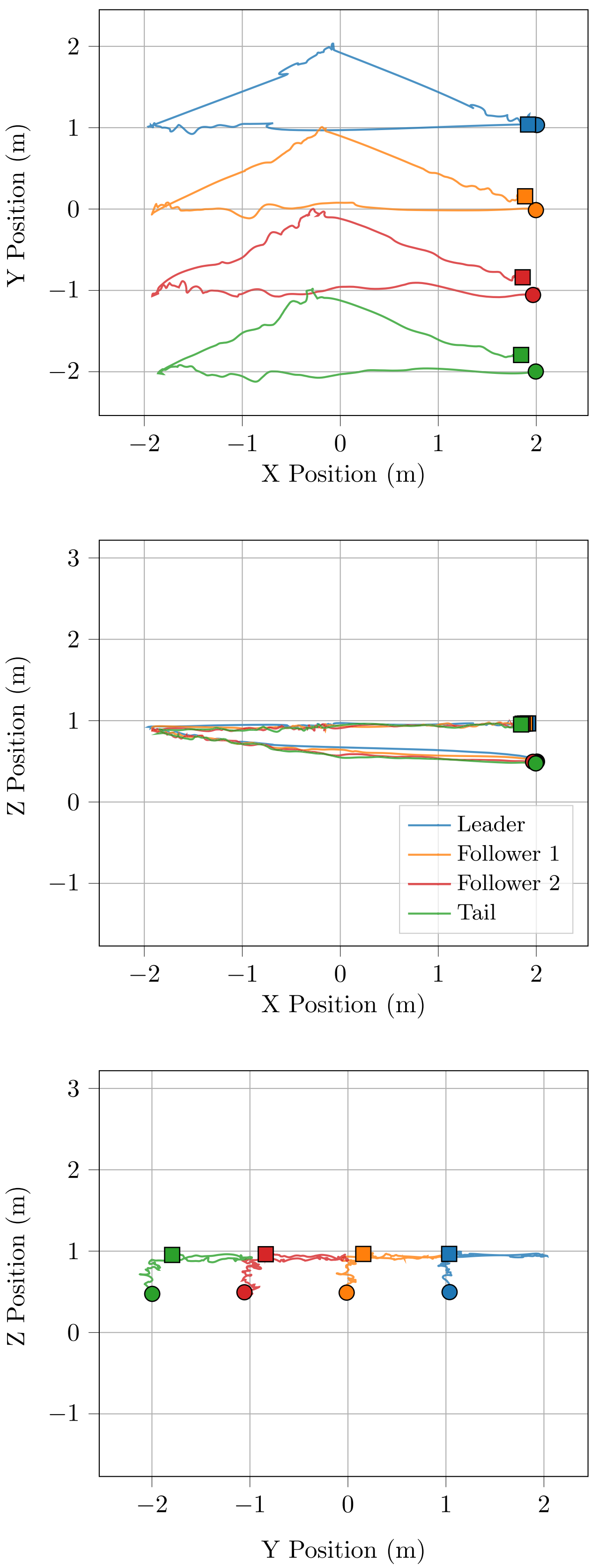

Fig. 12. Trajectories projected onto the XY (top), XZ (side), and YZ (front) planes. Start and end points are marked. The Tail drone exhibits reduced oscillations and enhanced stability.

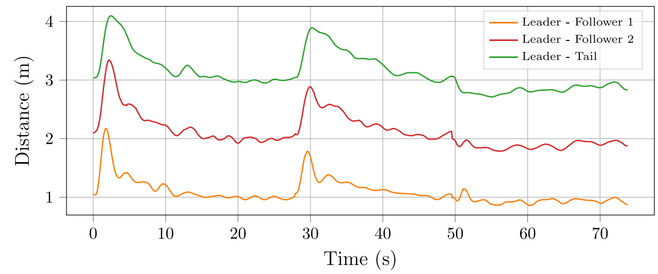

Fig. 13. Inter-agent distances from the leader to each follower as a function of time. Despite the leader's abrupt trajectory variations, the relative distances remain bounded and well-regulated. The damping agent, positioned at the tail, exhibits the lowest oscillatory amplitude, empirically validating its role in suppressing disturbance propagation and enhancing transient robustness within the formation.

8. Conclusion

In this work, we proposed a decentralized control protocol for formation tracking in multi-agent systems based on second-order dynamics with damping. The method introduces a spectral tuning approach that leverages a scalar parameter κ to regulate inter-agent coupling strength, enabling the design of controllers that are both asymptotically stable and capable of achieving fast convergence. By analyzing the closed-loop system through a Lyapunov framework, we established constraints on κ to guarantee bounded formation error, and we identified a design methodology to optimize performance while preserving stability.

We further investigated the robustness of the proposed protocol under switching topologies and communication failures. By deriving sufficient conditions based on dwell time and minimal connectivity eigenvalues, we showed that stability is preserved even when links fail or the graph structure changes, provided changes are not arbitrarily frequent. This theoretical robustness was validated through a spectral margin bound derived from the system's characteristic polynomial.

Experimental validation was carried out on a physical quadrotor swarm in the Drones Arena at the University of Trieste. The results confirmed the theoretical findings: the use of damping agents effectively mitigates high-frequency transients, enhances convergence behavior, and ensures persistent formation cohesion. The system performed robustly under trajectory perturbations and inter-agent delays, demonstrating the practical viability of the protocol in real-world decentralized scenarios.

Future work may extend the framework to heterogeneous agents, dynamic graph structures without dwell-time assumptions, and integration with learning-based estimation or fault recovery mechanisms.

CRediT authorship contribution statement

Erica Salvato: Writing – review & editing, Writing – original draft, Validation, Supervision, Methodology, Investigation, Funding acquisition, Formal analysis, Data curation, Conceptualization. **Alberto Trevisan:** Writing – original draft, Visualization, Validation, Software, Investigation. **Franco Blanchini:** Writing – review & editing, Writing – original draft, Methodology, Investigation, Conceptualization. **Felice Andrea Pellegrino:** Writing – review & editing, Writing – original draft, Visualization, Validation, Supervision, Methodology. **Gianfranco Fenu:** Writing – review & editing, Writing – original draft, Visualization, Validation.

Declaration of competing interest

The authors declare the following financial interests/personal relationships which may be considered as potential competing interests: Erica Salvato reports financial support was provided by European Union. If there are other authors, they declare that they have no known competing financial interests or personal relationships that could have appeared to influence the work reported in this paper.

Data availability

No data was used for the research described in the article.

References

[1] A. Dorri, S.S. Kanhere, R. Jurdak, Multi-agent systems: A survey, IEEE Access 6 (2018) 28573–28593.
[2] H.-S. Ahn, Formation Control, Springer, 2020.
[3] W. Levine, M. Athans, On the optimal error regulation of a string of moving vehicles, IEEE Trans. Autom. Control 11 (3) (1966) 355–361.
[4] Z. Sun, Cooperative Coordination and Formation Control for Multi-agent Systems, in: Springer Theses, Springer, 2018.
[5] W. Ren, Y. Cao, Distributed Coordination of Multi-Agent Networks: Emergent Problems, Models, and Issues, Springer Science & Business Media, 2010.
[6] M. de Queiroz, X. Cai, M. Feemster, Formation Control of Multi-Agent Systems: A Graph Rigidity Approach, in: Wiley Series in Dynamics and Control of Electromechanical Systems, John Wiley & Sons, Hoboken, NJ, USA, 2019.
[7] G. Lafferriere, A. Williams, J. Caughman, J. Veerman, Decentralized control of vehicle formations, Systems Control Lett. 54 (9) (2005) 899–910.
[8] K.-K. Oh, M.-C. Park, H.-S. Ahn, A survey of multi-agent formation control, Automatica 53 (2015) 424–440.
[9] T.H. Do, T.H. Hua, M.T. Nguyen, C.V. Nguyen, H.T.T. Nguyen, H.T. Nguyen, N.T.T. Nguyen, Formation control algorithms for multiple-UAVs: A comprehensive survey, EAI Endorsed Trans. Ind. Netw. Intell. Syst. 8 (27) (2021) e3.
[10] M.M. Alam, M.Y. Arafat, S. Moh, J. Shen, Topology control algorithms in multi-unmanned aerial vehicle networks: An extensive survey, J. Netw. Comput. Appl. 207 (2022) 103495.
[11] X. Zhang, Q. Yang, F. Xiao, H. Fang, J. Chen, Linear formation control of multi-agent systems, Automatica 171 (2025) 111935.
[12] F. Mehdifar, C.P. Bechlioulis, F. Hashemzadeh, M. Baradarannia, Prescribed performance distance-based formation control of multi-agent systems, Automatica 119 (2020) 109086.
[13] W. Ren, R.W. Beard, E.M. Atkins, Information consensus in multivehicle cooperative control, IEEE Control Syst. Mag. 27 (2) (2007) 71–82.
[14] W. Ren, Consensus based formation control strategies for multi-vehicle systems, in: 2006 American Control Conference, IEEE, 2006, pp. 6–pp.
[15] J.R. Lawton, R.W. Beard, B.J. Young, A decentralized approach to formation maneuvers, IEEE Trans. Robot. Autom. 19 (6) (2004) 933–941.
[16] G. Xie, L. Wang, Consensus control for a class of networks of dynamic agents, Int. J. Robust Nonlinear Control.: IFAC-Affiliated J. 17 (10–11) (2007) 941–959.
[17] Y. Cao, W. Ren, Distributed coordination of fractional-order systems with extensions to directed dynamic networks and absolute/relative damping, in: Proceedings of the 48h IEEE Conference on Decision and Control (CDC) Held Jointly with 2009 28th Chinese Control Conference, IEEE, 2009, pp. 7125–7130.
[18] G. Giordano, Structural Analysis and Control of Dynamical Networks (Ph.D. thesis), Università degli Studi di Udine, 2016.
[19] G. Giordano, M. Segata, F. Blanchini, R. Lo Cigno, A joint network/control design for cooperative automatic driving, in: 9th IEEE Vehicular Networking Conference, VNC 2017, IEEE, Torino, Italy, 2017, pp. 167–174.
[20] G. Giordano, M. Segata, F. Blanchini, R. Lo Cigno, The joint network/control design of platooning algorithms can enforce guaranteed safety constraints, Ad Hoc Netw. 94 (2019).
[21] F. Bullo, Lectures on Network Systems, 1.7 ed., Kindle Direct Publishing, 2024.
[22] G. Giordano, F. Blanchini, E. Franco, V. Mardanlou, P.L. Montessoro, The smallest eigenvalue of the generalized Laplacian matrix, with application to network-decentralized estimation for homogeneous systems, IEEE Trans. Netw. Sci. Eng. 3 (4) (2016) 312–324.
[23] X. Zhou, H. Sun, W. Li, Z. Zhang, Optimization on the smallest eigenvalue of grounded Laplacian matrix via edge addition, Theoret. Comput. Sci. 980 (2023).
[24] M. Pirani, S. Sundaram, On the smallest eigenvalue of grounded Laplacian matrices, IEEE Trans. Autom. Control 61 (2) (2016).
[25] R. Rajamani, Vehicle Dynamics and Control, second ed., 2012.
[26] A. Ali, G. Garcia, P. Martinet, The flatbed platoon towing model for safe and dense platooning on highways, IEEE Intell. Transp. Syst. Mag. 7 (1) (2015) 58–68.
[27] J.C. Zegers, E. Semsar-Kazerooni, J. Ploeg, N. van de Wouw, H. Nijmeijer, Consensus-based bi-directional CACC for vehicular platooning, in: American Control Conference (ACC 2016), Boston, MA, 2016, pp. 2578–2584.
[28] S. Santini, A. Salvi, A.S. Valente, A. Pescapé, M. Segata, R. Lo Cigno, A consensus-based approach for platooning with inter-vehicular communications and its validation in realistic scenarios, IEEE Trans. Veh. Technol. 66 (3) (2017) 1985–1999.
[29] S. Oncu, J. Ploeg, N. Van De Wouw, H. Nijmeijer, Cooperative adaptive cruise control: Network-aware analysis of string stability, IEEE Trans. Intell. Transp. Syst. 15 (4) (2014) 1527–1537.
[30] M. Segata, R. Lo Cigno, Automatic emergency braking - realistic analysis of car dynamics and network performance, IEEE Trans. Veh. Technol. 62 (9) (2013) 4150–4161.
[31] M. Segata, S. Joerer, B. Bloessl, C. Sommer, F. Dressler, R. Lo Cigno, PLEXE: A platooning extension for veins, in: 6th IEEE Vehicular Networking Conference, VNC 2014, Paderborn, Germany, 2014, pp. 53–60.
[32] D. Liberzon, Switching in Systems and Control, Birkhäuser, 2003.